2014

Pressure Drop in Condensing Superheated Zone

Melissa Meyer
Air Conditioning and Refrigeration Center, University of Illinois at Urbana-Champaign, mcmeyer4@illinois.edu

Predrag S. Hrnjak
pega@illinois.edu

Pressure Drop in Condensing Superheated Zone

Melissa MEYER[1], Pega HRNJAK[1,2*]

[1] University of Illinois at Urbana-Champaign,
Department of Mechanical Science and Engineering,
Urbana, Illinois, USA
mcmeyer4@illinois.edu, pega@illinois.edu

[2]Creative Thermal Solutions,
Urbana, Illinois, USA

* Corresponding Author

ABSTRACT

Traditionally, condensation is characterized by division into three zones: desuperheating, condensation and subcooling. It was shown that condensation starts even in the presence of superheated vapor, when the wall temperature reaches saturation. Heat transfer effects of that process were described earlier but not pressure drop that was later found to indicate the presence of condensate, the same as shown by heat transfer results. Pressure drop in condensers has traditionally been modeled separately for single-phase and two-phase regions. When plotted as a function of enthalpy, the correlations show a discontinuity between the single-phase and two-phase zones because the models typically assume thermodynamic equilibrium during condensation. This assumption indicates that the first drop or film of condensate would form when the bulk refrigerant enthalpy reached the saturated vapor enthalpy. In reality, condensation starts when the wall temperature reaches the saturation temperature even if the bulk enthalpy is still indicating a superheated state. That makes a fourth zone in the condenser: it begins when the wall temperature reaches the saturation temperature and ends when the bulk enthalpy reaches saturated vapor, and is classified as the condensing superheated zone. In this condensing superheated zone, the interaction between the condensate film and vapor increases the pressure drop compared to vapor alone. This paper presents experimental results for pressure drop in that zone of the condenser for R32, R134a and R1234ze(E). The pressure drop was found to be higher than predicted by single-phase correlations such as Colburn (1933).

1. INTRODUCTION

Traditionally, condensation has been described using three zones: desuperheating, two-phase, and subcooled regions. The two-phase region begins when the bulk enthalpy of the condensing fluid reaches the saturated vapor enthalpy, and ends when the bulk enthalpy reaches the saturated liquid value. This approach implicitly assumes thermodynamic equilibrium throughout the condensation process. In reality, the refrigerant is not at equilibrium, and condensation occurs outside the conventionally defined two-phase zone.

The disadvantage of characterizing condensation heat transfer and pressure drop by the three zones listed above is that the models give unrealistic predictions at the boundaries of the zones. When plotted as a function of enthalpy, the correlations for heat transfer coefficient and pressure drop show discontinuities between the single-phase and two-phase regions, as seen in figure 1. These discontinuities occur due to the assumption of thermodynamic equilibrium, which indicates that the first drop of condensate would form when the bulk refrigerant enthalpy reached the saturated vapor enthalpy, i.e. at the start of the two-phase zone. However, the refrigerant has a nonuniform temperature profile across the diameter of the tube, and the fluid is colder in the vicinity of the wall than in the center of the tube. Experimental studies have indicated that condensation begins when the wall temperature falls below the saturation temperature, even in the presence of superheated vapor in the center of the tube. Similarly, condensation continues when the bulk enthalpy of the refrigerant is less than the saturated liquid enthalpy, in the presence of some subcooled liquid.

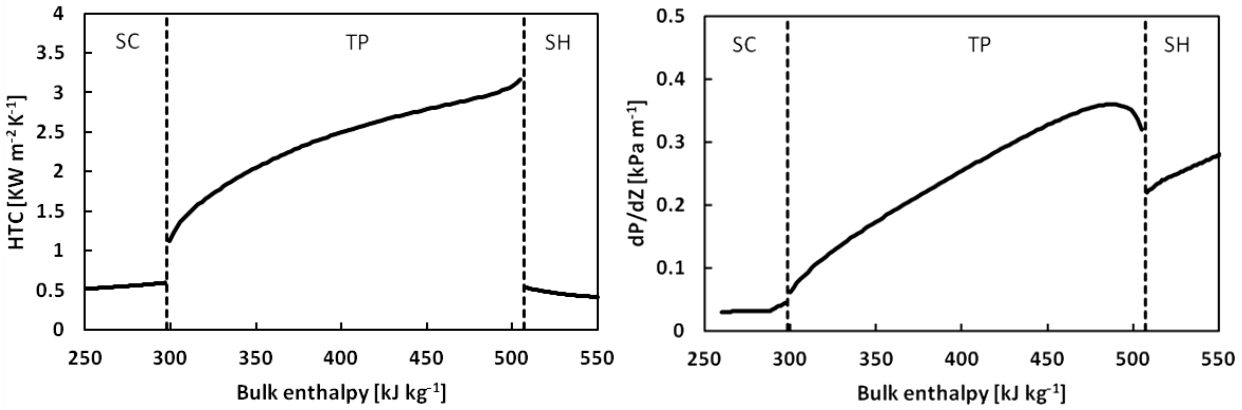

Figure 1: Traditional condensation models for heat transfer coefficient and pressure drop with subcooled, two-phase, and superheated regions. The plots shown are for R32 at 3.141 MPa with a mass flux of 100 kg m^{-2} s^{-1}. The example correlations shown are those of Cavallini (2006) for two-phase HTC, Gnielinski (1976) for single-phase HTC, Friedel (1979) for two-phase pressure drop, and Colburn (1933) for single-phase pressure drop.

The heat transfer effects of these processes have been described earlier by Kondou and Hrnjak (2011a, 2011b, 2012) and by Agarwal and Hrnjak (2013). They defined a total of five zones: desuperheating, condensing superheated, two-phase, condensing subcooled, and subcooled regions. The condensing superheated zone begins when the wall temperature reaches the saturation temperature. The two-phase zone is defined as before, as the region in which the bulk enthalpy is saturated. The condensing subcooled region begins at the saturated liquid enthalpy and ends when all of the vapor has condensed. In the condensing superheated and condensing subcooled zones, condensation increases the heat transfer coefficient above the single-phase correlation predictions so that it transitions smoothly between the two-phase and single-phase regions, as shown in figure 2. Kondou and Hrnjak (2012) proposed a correlation combining the single-phase and two-phase heat transfer coefficients to predict the heat transfer coefficient in the condensing superheated zone. However, the pressure drop in that zone has not yet been described.

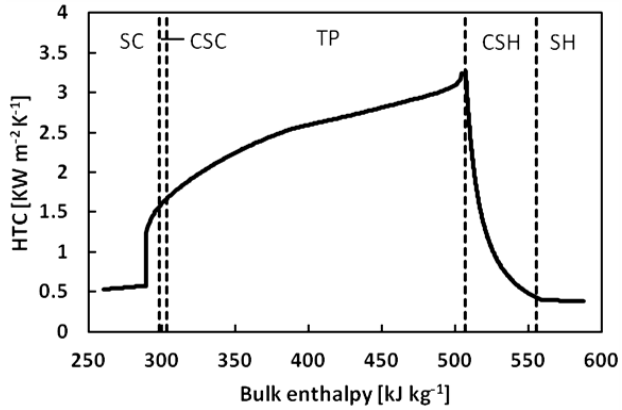

Figure 2: Five-zone condensation model for R32 at 3.141 MPa with a mass flux of 100 kg m^{-2} s^{-1}. The example correlations shown are those of Cavallini (2006) for two-phase and condensing subcooled regions, Gnielinski (1976) for desuperheating and subcooled regions, and Kondou-Hrnjak (2012) for the condensing superheated region.

2. EXPERIMENTAL SETUP

2.1 Experimental facility

Figure 3 shows a schematic of the facility in which experiments were performed to measure both the heat transfer and pressure drop of condensing refrigerants. The apparatus includes separate loops for refrigerant, water, and chilled water. The refrigerant loop consists of a variable speed gear pump, a coriolis-type mass flow meter, an electric pre-heater, a mixing chamber, a counter-flow concentric tube pre-cooler, a test section, sight glass, two after-coolers, and a receiver tank. A diaphragm-type differential pressure transducer measures the separate pressure

drops across the pre-cooler and the test section. The pressure is controlled by the refrigerant charge, heater setting, and flow rate of chilled water through the after-coolers. The refrigerant flow rate is controlled by the gear pump. The refrigerant is initially superheated in the pre-heater, and its condition at the test section inlet is adjusted by the temperature and flow rate of water through the pre-cooler. The heat flux in the test section is controlled by the flow of water through the test section.

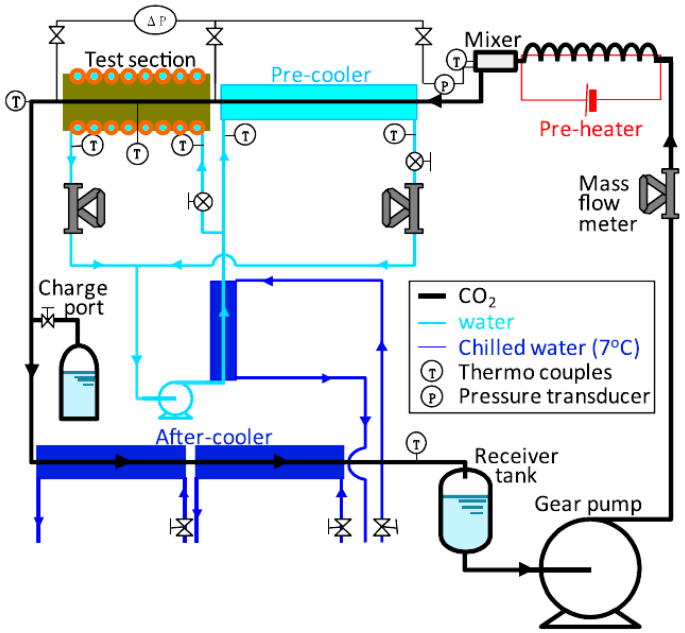

Figure 3: Schematic of experimental facility (Kondou and Hrnjak, 2011a)

2.2 Test section

Figure 4 illustrates the test section, which consists of a smooth copper tube 150 mm long with inner and outer diameters of 6.1 mm and 9.53 mm, respectively. The tube is oriented horizontally and covered with a thick brass jacket, with thermal paste filling the gap between the tube and jacket. Water flows through copper tubes soldered around the outside of the brass jacket, producing uniform cooling conditions throughout the test section. Twelve thermocouples are embedded in the top, bottom, left, and right of the test tube wall at three axial positions. Just before and after the test section, two 1.0-mm holes are bored through the refrigerant tube wall as pressure ports and connected to a differential pressure transducer through capillary tubes. The length between the pressure ports is 288 mm.

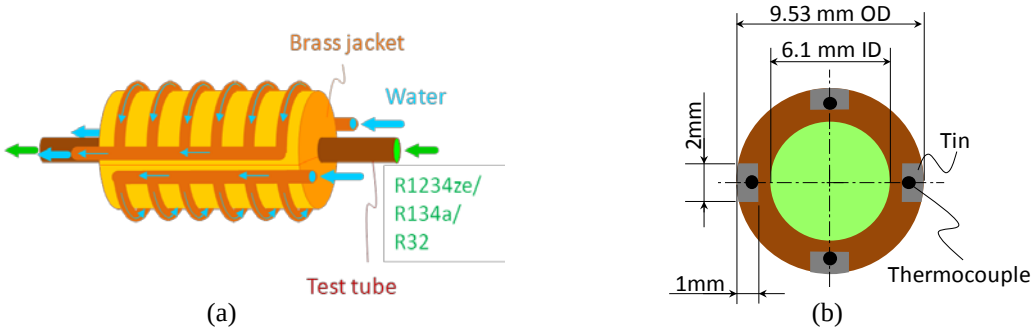

Figure 4: (a) Test section with fluid flow directions (b) Cross-section of test tube (Kondou and Hrnjak, 2011b)

2.3 Measurements and data reduction

The instruments used and uncertainties of experimental measurements are summarized in table 1. The refrigerant temperature and pressure are measured in the mixer and the enthalpy is calculated under the assumption of equilibrium using Refprop 8.0 (Lemmon *et al.*, 2007). The changes in enthalpy over the pre-cooler and test section

are obtained from water-side energy balances using the measured mass flow rates and inlet and outlet water temperatures, according to equations (1) and (2):

$$\Delta h_{PC} = \left[\left(T_{H2O,PCo} - T_{H2O,PCi}\right)\dot{m}_{H2O,PC} c_{pH2O} - \dot{Q}_{gain,PC}\right]/\dot{m}_r \quad (1)$$

$$\Delta h_{TS} = \left[\left(T_{H2O,TSo} - T_{H2O,TSi}\right)\dot{m}_{H2O,TS} c_{pH2O} - \dot{Q}_{gain,TS}\right]/\dot{m}_r \quad (2)$$

where $\dot{Q}_{gain,PC}$ and $\dot{Q}_{gain,TS}$ are preliminarily-measured heat leaks to ambient air through the insulation. The bulk mean temperature of the refrigerant in the test section is calculated from the bulk enthalpy and pressure with Refprop's equilibrium state function, as shown in equations (3)-(5).

$$T_{rb,i} = f_{equilibrium}\left(h_{b,MC} - \Delta h_{PC},\ P_{MC} - \Delta P_{PC}\right) \quad (3)$$

$$T_{rb,o} = f_{equilibrium}\left(h_{b,MC} - \Delta h_{PC} - \Delta h_{TS},\ P_{MC} - \Delta P_{PC} - \Delta P_{TS}\right) \quad (4)$$

$$T_{rb} = \left(T_{rb,i} + T_{rb,o}\right)/2 \quad (5)$$

The average heat flux on the interior wall of the test section is given by equation (6):

$$q_{wi} = \left[\left(T_{H2O,TSo} - T_{H2O,TSi}\right)\dot{m}_{H2O,TS} c_{pH2O} - \dot{Q}_{gain,TS} - \dot{Q}_{cond}\right]/(\pi d_i L) \quad (6)$$

where $\dot{Q}_{cond}$ is heat conducted from upstream of the test section, numerically estimated for each set of test conditions. The average heat transfer coefficient is defined by equation (7):

$$HTC = q_{wi}/\left(T_{rb} - T_{wi}\right) \quad (7)$$

where T_{wi} is the average of the twelve temperature measurements in the wall of the test section. The average pressure drop gradient is defined by equation (8):

$$dP/dZ = \Delta P_{TS}/\Delta Z \quad (8)$$

where ΔZ is the distance between the pressure ports. The measurements and data reduction procedure are illustrated in figure 5.

The uncertainties listed in table 1 are obtained from two standard deviations of calibration, the resolution of calibration equipment and data loggers, and the stability of excitation voltages. The combined uncertainties are calculated according to ASME Performance Test Codes (1985) and Moffat (1988) and are shown as error bars in the plots below.

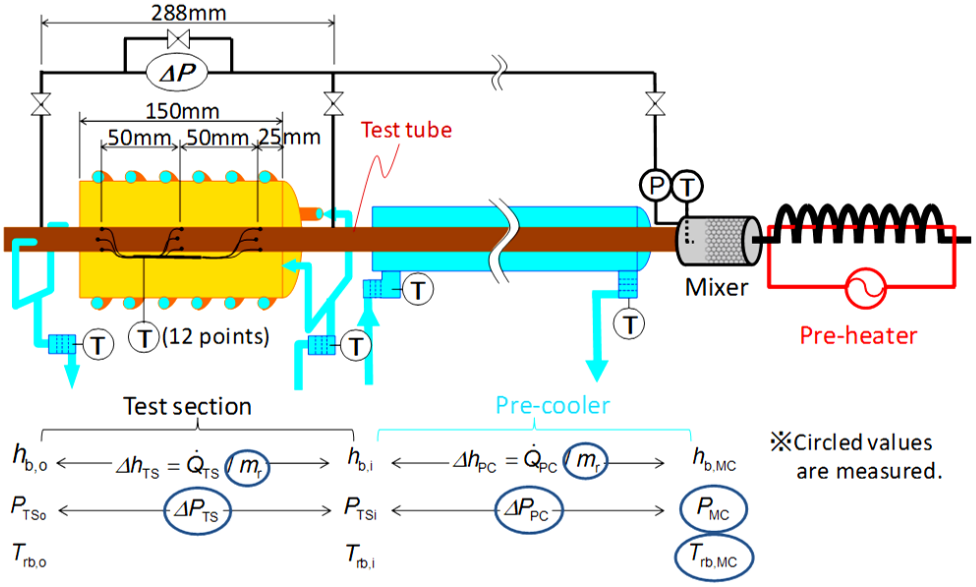

Figure 5: Measurement locations and data reduction procedure (Kondou and Hrnjak, 2011b)

Table 1: Measurement uncertainties

Measured variable	Instrument	Uncertainty
T_{rb}, T_{H2O}	Sheathed T-type thermocouple	±0.05 K
T_{wi}	Twisted T-type thermocouple	±0.16 K
P_{MC}	Diaphragm absolute pressure transducer	±4 kPa
ΔP	Diaphragm differential pressure transducer	±0.13 kPa
$\dot{m}_{H2O,TS}$, $\dot{m}_r$	Coriolis mass flow meter	±0.1 g/s
$\dot{m}_{H2O,PC}$	Coriolis mass flow meter	±0.5 g/s

3. RESULTS AND DISCUSSION

3.1 Identification of condensing superheated zone

Figure 6 shows experimental results for R32 at a pressure of 3.141 MPa (corresponding to a saturation temperature of 50 °C), a mass flux of 300 kg m^{-2} s^{-1}, and a heat flux of 10 kW m^{-2}. Examples of two-phase and single-phase heat transfer and pressure drop correlations are shown along with the experimental data points. The dashed vertical lines indicate the boundaries of the condensing superheated zone. This zone is identified using the experimentally measured temperatures shown in figure 6c. The condensing superheated zone begins when the test section wall temperature falls below the saturation temperature. At that point, condensation begins and is indicated by the sharp rise in heat transfer coefficient and pressure drop gradient, as seen in figures 6a and 6b. However, the bulk refrigerant temperature at the test section is still superheated and drops from the inlet to the outlet, as seen in figure 6c, due to continuing sensible heat transfer. Once the bulk refrigerant reaches saturated vapor conditions, it enters the two-phase zone and there is primarily latent heat transfer. Further heat transfer results are presented by Kondou and Hrnjak (2011a, 2011b, 2012) and by Agarwal and Hrnjak (2013) and show similar behavior demonstrating the existence of a condensing superheated region.

3.2 Pressure drop in condensing superheated zone

In the desuperheating zone, the experimental pressure drop generally tends to decrease as the bulk enthalpy decreases due to the reduction in specific volume and thus velocity, as predicted by the Colburn (1933) correlation. However, rather than continuing to follow that trend in the condensing superheated region, the pressure drop increases as the bulk enthalpy decreases once condensation begins. In the two-phase region, the experimental pressure drop follows the general trend predicted by the Friedel (1979) correlation, first increasing to a maximum at a quality of about 0.92 and then decreasing as the enthalpy decreases further, as seen in figure 6b.

The pressure drop is higher than predicted by the Colburn (1933) correlation in the condensing superheated zone because the single-phase model does not take into account the shear interactions between the vapor and the liquid film that begins to form as condensation starts before the two-phase region. The energy dissipated by these interactions leads to an escalation in pressure drop. The phenomenon is indicated by the Friedel (1979) correlation, which predicts an initial increase in pressure drop during the early stages of condensation. However, the Friedel (1979) correlation, applied only in the two-phase region, shows the rise in pressure drop beginning too late. The causes for the observed trend are therefore accepted already but have been assumed to be relevant only in the two-phase region, when actually they should be considered as soon as condensation starts in the condensing superheated zone. The assumptions about the appearance of condensate under the three-zone and five-zone models are illustrated in figure 7.

The pressure drop begins to rise at the beginning of condensation as enough liquid condenses to form a film all around the tube. As condensation continues and the liquid film thickens, more waves can form and increase the shear at the liquid-vapor interface, further increasing the pressure drop. Simultaneously however, the density of the refrigerant is increasing, so the velocity is decreasing with a constant mass flux. The refrigerant density and velocity are shown as functions of specific enthalpy in figure 6d, assuming no slip. As the velocity decreases, friction and momentum loss from the refrigerant are reduced. The peak and subsequent decrease in pressure drop as condensation progresses may be caused by the reduction of velocity enough to offset the effect of the thicker, wavier film. The pressure drop pattern may also be produced by a change in the flow regime at a quality around 0.92. The authors are conducting flow visualization experiments to determine how the refrigerant flow develops as condensation occurs and to clarify the underlying causes for the observed pressure drops.

3.3 Comparison of pressure drop for various fluids and test conditions

Figures 8a, 8b, and 8c show experimental results for R32, R134a, and R1234ze(E) at a saturation temperature of 50 °C, mass flux of 300 kg m^{-2} s^{-1}, and heat flux of 10 kW m^{-2}. Figure 8d shows the results for R1234ze(E) at the same saturation temperature and heat flux but with a mass flux of 200 kg m^{-2} s^{-1}. R32, R134a, and R1234ze(E) have pressures of 3.141 MPa, 1.319 MPa, and 0.997 MPa, respectively, at a saturation temperature of 50 °C. As seen in figure 8, the lower-pressure fluids have significantly higher pressure drop than R32 at the same saturation temperature. For the same fluid, R1234ze(E), figures 8c and 8d show that the pressure drop is higher for a higher mass flux. Higher mass flux indicates higher fluid velocity and thus greater friction as well as greater momentum loss from the fluid. However, the basic trends of the pressure drop in each zone are similar for each fluid and mass flux. In each case, the pressure drop displays the general pattern discussed above: decreasing in the desuperheating region, increasing in the condensing superheated region, peaking and then diminishing in the two-phase region as the bulk enthalpy decreases.

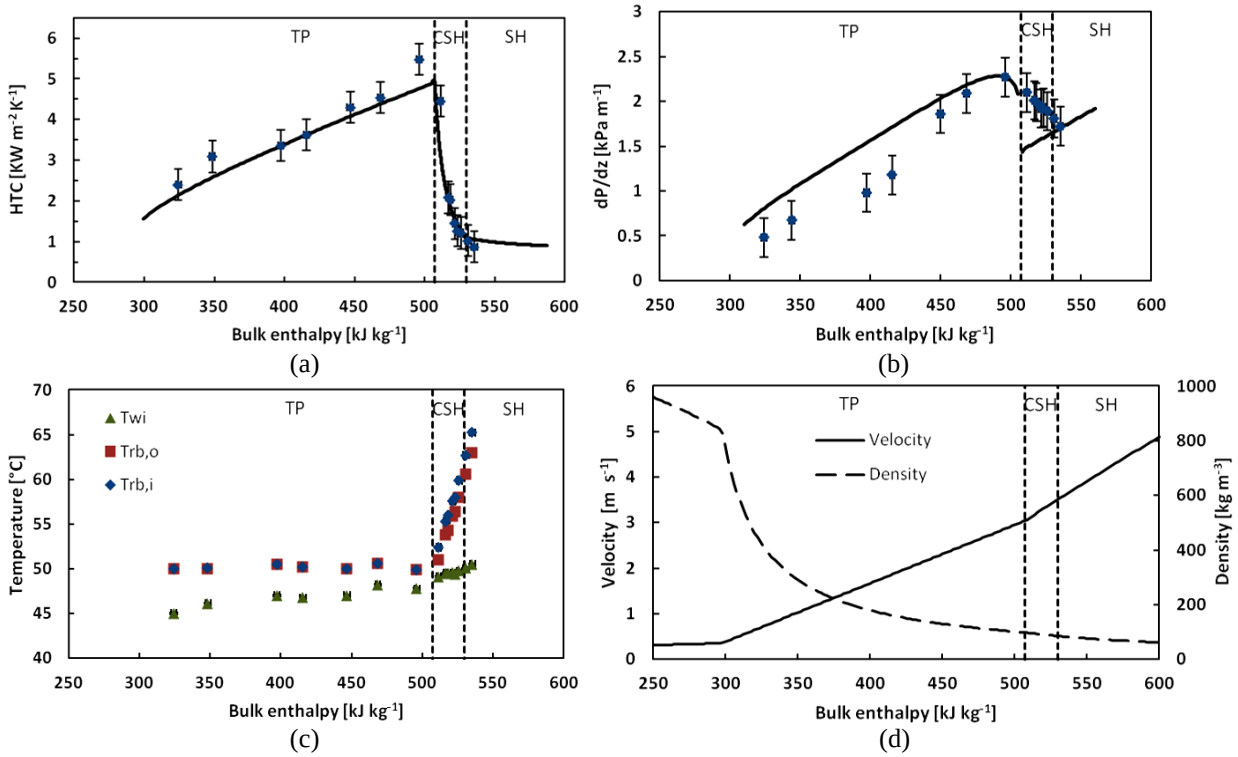

Figure 6: R32 at 3.141 MPa (T_{sat} = 50°C) and 300 kg m^{-2} s^{-1}: (a) Heat transfer coefficient experimental data with Cavallini (2006), Kondou-Hrnjak (2012), and Gnielinski (1976) correlations (b) Pressure drop experimental data with Friedel (1979) and Colburn (1933) correlations (c) Test section wall and refrigerant temperatures (d) No-slip model predictions for refrigerant velocity and density

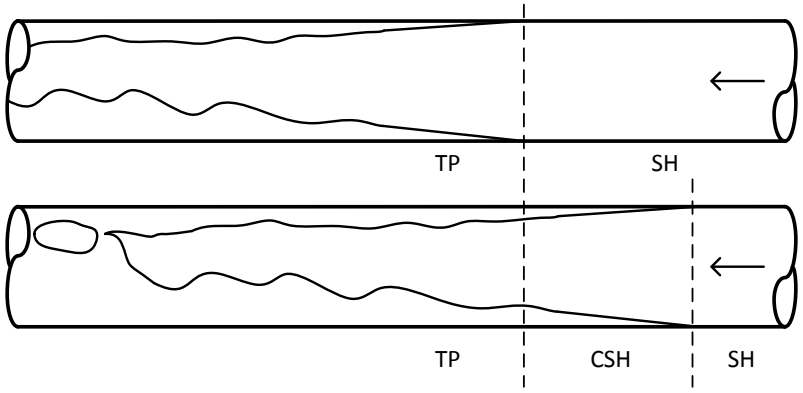

Figure 7: Simplified representations of how condensate is assumed to form with a conventional three-zone model (top) and a five-zone model including the condensing superheated zone (bottom)

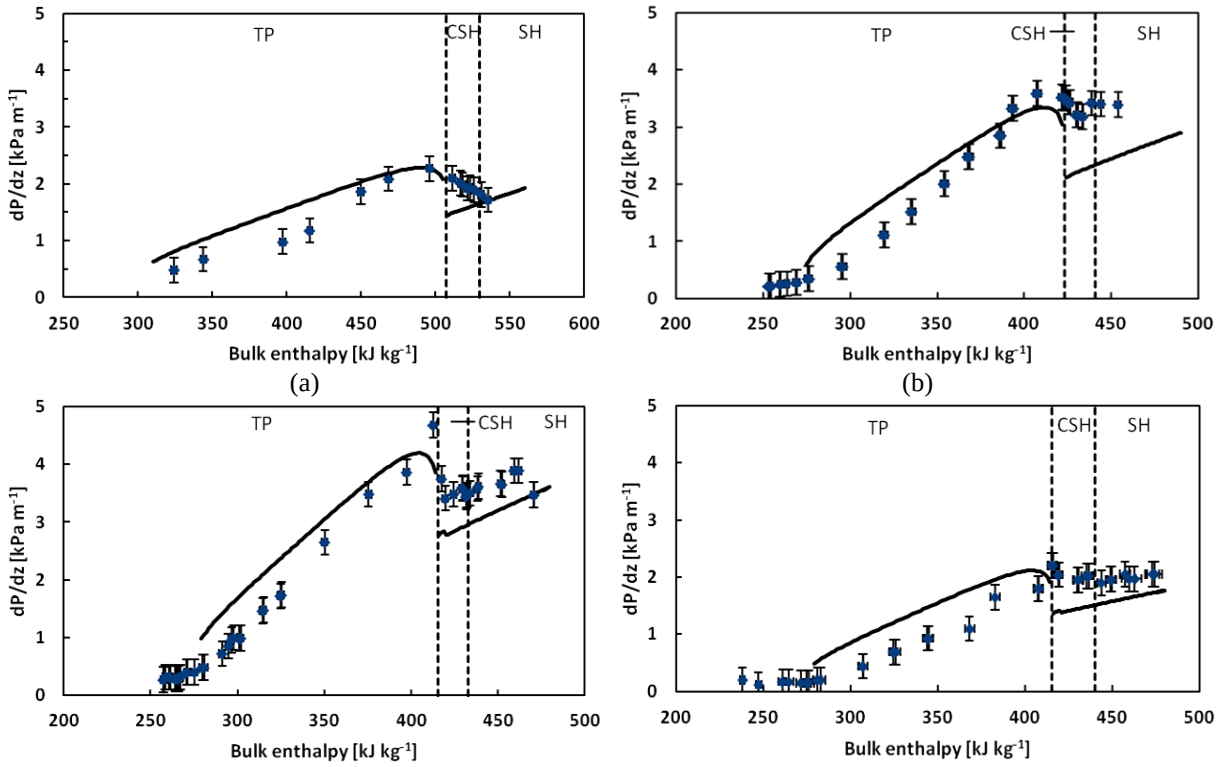

Figure 8: Pressure drop experimental data with Friedel (1979) and Colburn (1933) correlations: (a) R32 at 3.141 MPa (T_{sat} = 50°C) and 300 kg m^{-2} s^{-1} (b) R134a at 1.319 MPa (T_{sat} = 50°C) and 300 kg m^{-2} s^{-1} (c) R1234ze(E) at 0.997 MPa (T_{sat} = 50°C) and 300 kg m^{-2} s^{-1} (d) R1234ze(E) at 0.997 MPa (T_{sat} = 50°C) and 200 kg m^{-2} s^{-1}

4. CONCLUSIONS

Experimental pressure drop results have been presented for R32, R134a, and R1234ze(E) condensing in a horizontal smooth tube. As the enthalpy decreases in the superheated region, the pressure drop also tends to decline as predicted by single-phase correlations such as Colburn (1933). However, the experimental pressure drop deviates from the single-phase correlation prior to the saturated vapor point. This deviation is due to the presence of condensate as soon as the tube wall temperature falls below the saturation temperature, even while the bulk refrigerant enthalpy is superheated. In this condensing superheated region, the interaction of the condensate film with the vapor increases the pressure drop compared to what is expected for vapor alone. The pressure drop gradient then reaches a peak early in the two-phase region and decreases as predicted by the Friedel (1979) correlation.

NOMENCLATURE

c_p	Specific heat capacity	(J kg^{-1} K^{-1})
d_i	Inner diameter of test tube	(m)
h	Specific enthalpy	(J kg^{-1})
HTC	Heat transfer coefficient	(W m^{-2} K^{-1})
L	Cooling length of test tube	(m)
$\dot{m}$	Mass flow rate	(kg s^{-1})
P	Pressure	(Pa)
$\dot{Q}$	Heat transfer rate	(W)
q	Heat flux	(W m^{-2})
T	Temperature	(°C)
Z	Distance along test tube	(m)
ρ	Density	(kg m^{-3})

Subscripts

b	Evaluated at bulk temperature
cond	Conduction heat from upstream
gain	Heat gain from ambient air
H2O	Water
i	Inlet
MC	Mixing chamber
o	Outlet
PC	Pre-cooler
r	Refrigerant
sat	Saturated
TS	Test section
wi	Inner wall of test section

REFERENCES

Agarwal, R., Hrnjak, P., 2013, Condensation in two phase and desuperheating zone for R1234ze(E), R134a and R32 in horizontal smooth tubes, *Int. J. Refrigeration*, in print.

ASME Performance Test Codes, 1985, Supplement on Instruments & Apparatus, P.1, *ANSI/ASME PTC*: 19.1-1985.

Cavallini, A., Del Col, D., Doretti, L., Matkovic, M., Rossetto, L., Zilio, C., Censi, G., 2006, Condensation in horizontal smooth tubes: a new heat transfer model for heat exchanger design, *Heat Tran. Eng.*, vol. 27, no. 8: p. 31-38.

Colburn, A.P., 1933, A method of correlating forced convection heat transfer data and comparison with fluid friction, *Trans. AIChE*, vol. 29, p. 174-210.

Friedel, L., 1979, Improved friction pressure drop correlations for horizontal and vertical two phase pipe flow, *Proc. European Two-Phase Flow Group Meeting*, Ispra, Italy, Paper No. E2.

Gnielinski, V., 1976, New equation of heat and mass transfer in turbulent pipe and channel flow, *Int. Chem. Eng.*, vol. 16, p. 359-367.

Kondou, C., Hrnjak, P., 2011a, Heat rejection from R744 flow under uniform temperature cooling in a horizontal smooth tube around the critical point, *Int. J. Refrigeration*, vol. 34, no. 3, p. 719-731.

Kondou, C., Hrnjak, P., 2011b, Heat rejection in condensers close to critical point-desuperheating, condensation in superheated region and condensation of two phase fluid, *Int. Conf. Heat Trans. Fluid Mech. and Thermodynamics*, Mauritius.

Kondou, C., Hrnjak, P., 2012, Condensation from superheated vapor flow of R744 and R410A at subcritical pressures in a horizontal smooth tube, *Int. J. Heat Mass Transfer*, vol. 55, p. 2779-2791.

Lemmon, E.W., Huber, M.L., McLinden, M.O., 2007, Reference Fluid Thermodynamic and Transport Properties-REFPROP Ver.8.0, National Institute of Standards and Technology, Boulder, CO, USA.

Moffat, R.J., 1988, Describing the uncertainties in experimental results, *Exp. Therm. Fluid Sci*., vol. 1, p. 3-17.

ACKNOWLEDGEMENT

The authors gratefully acknowledge the financial support of the Air Conditioning and Refrigeration Center (ACRC) at the University of Illinois at Urbana-Champaign.